# Characterizations of Transparent Polyimide Nanocomposite Films with Various Equibiaxial Stretching Ratios: Optical Transparency, Morphology, and Oxygen Permeability

**Ungki Min,[1] Choon Sup Yoon,[2] Jin-Hae Chang[1]**

[1]*School of Energy and Integrated Materials Engineering, Kumoh National Institute of Technology, Gumi 730-701, Korea*
[2]*Department of Physics, Korea Advanced Institute of Science and Technology, Daejeon 305-701, Korea*

Received 16 May 2011; accepted 23 July 2011
DOI 10.1002/app.35368
Published online in Wiley Online Library (wileyonlinelibrary.com).

**ABSTRACT:** A series of transparent polyimide (PI) nanocomposite films was synthesized from bicyclo(2,2,2)oct-7-ene-2,3,5,6-tetracarboxylic dianhydride and 1,3-bis(3-aminophenoxy) benzene with various organoclay contents via solution intercalation polymerization to poly(amic acid)s, followed by thermal imidization. Varying the organoclay loading in the range 0–1.5 wt % produced variations in the optical transparency, morphology, and oxygen barrier properties of the hybrids. The optimum oxygen barrier properties were observed for the hybrids containing 1.0 wt % Cloisite 30B; these properties were degraded gradually by further increases in the clay content. The PI hybrid films were found to exhibit excellent optical transparency and to be almost colorless. However, the transparency of the hybrid films decreased slightly with increasing organoclay content. Transparent PI hybrid films containing 1.0 wt % Cloisite 30B were stretched equibiaxially with various stretching ratios in the range 100–140% to investigate their optical transparency and oxygen permeability in detail; the variations with equibiaxial stretching ratio of the clay dispersion and morphology were also determined. PI hybrid films with stretching of 120% or greater were found to contain homogeneously dispersed clay in the polymer matrix and exfoliated nanocomposites. The highest barrier to oxygen permeation was found to arise at an equibiaxial stretching ratio of 130%.  J Appl Polym Sci 000: 000–000, 2012

**Key words:** nanotechnology; organoclay; polyimides

## INTRODUCTION

Aromatic polyimides (PIs) are among the most important superengineering materials because they show excellent mechanical properties and thermal stability at elevated temperatures. These favorable characteristics are due to the presence of imide linkages in the polymer backbone. Aromatic PIs have been evaluated for use in microelectronics, aerospace, and military applications.[1–5] However, the yellowish quality of aromatic PIs, which is due to the highly conjugated aromatic structures and intermolecular and/or intramolecular charge-transfer complex formation by molecular interactions, limits their use in optical applications.[6–9]

Several approaches have been used to prepare colorless and transparent PIs, including the incorporation of kink linkages in the main chain to reduce linearity, the introduction of pendant groups onto the main chain to reduce molecular packing, and the introduction of strong electron-withdrawing side groups, such as fluorinated groups.[10–12] In general, the low cutoff wavelength ($\lambda_o$) and the colorless nature of these PI films can be attributed to the strong electron-withdrawing groups in the monomers, which inhibit charge-transfer complex formation and decrease intermolecular interactions.[13–15] However, progress in the preparation of colorless and transparent PI films largely relies on the design and synthesis of new PI monomers.[16–18]

The properties of organic–inorganic nanometer-scaled blended composites are superior to those of conventional composites because interfacial adhesion is maximized in the nanocomposites as a result of their nanometer dimensions. Materials incorporating polymer/clay hybrids can attain the desired stiffness, strength, and gas barrier properties with the addition of far less inorganic material than present in conventionally filled polymer composites. It has been found that the higher the degree of

*Correspondence to:* J.-H. Chang (changjinhae@hanmail.net).

Contract grant sponsor: Information Technology Research & Development Program of Ministry of Knowledge Economy; contract grant number: 2008-F024-01 (development of mobile flexible Input Output platform).

delamination in such polymer–clay hybrids is, the greater the enhancement of these properties will be.[19–21]

The permeability of a composite depends on several factors, including the quantity, length, and width of the clay particles, and their orientation and dispersion.[22,23] Numerous studies have shown that the aspect ratio of exfoliated clay particles plays a critical role in the control of the microstructure of polymer/clay nanocomposites and their gas barrier performance.[24–26] Although polymer/clay nanocomposites are known to exhibit gas barrier properties that are better than those of conventional composite systems, the dependence of these properties on factors such as the orientations of the matrix sheets and the extent of clay aggregation and dispersion (intercalation, exfoliation, or intermediate structures) is not well understood. Bharadwaj[27] constructed a model for the barrier properties in polymer-layered silicate nanocomposites based completely upon the tortuosity arguments described by Nielsen.[28] The correlations among sheet length, concentration, relative orientation, and aggregation state are expected to provide guidance in the design of better barrier materials with the nanocomposite approach.[29]

Biaxial orientation is achieved either by sequential biaxial stretching, in which a sheet is stretched in one direction and again in an orthogonal direction or by simultaneous or equibiaxial stretching, in which both axes are stretched simultaneously.[30] Several reports have described the effects of biaxial stretching on the crystallinity and morphological behaviors in a polymer matrix.[31–34] Jeol et al.[32] studied the effects of uniaxial and biaxial stretching on the dispersion of two types of silica nanocomposites in a poly(ethylene terephthalate) matrix. They found that high shear during preform injection molding created an isotropic composite morphology, as was evident from transmission electron microscopy (TEM) images.

In this study, we prepared a colorless PI through the reaction of bicyclo(2,2,2)oct-7-ene-2,3,5,6-tetracarboxylic dianhydride (BTDA) and 1,3-bis(3-aminophenoxy) benzene (BAPB) in *N,N*-dimethylacetamide (DMAc). Transparent PI hybrid films were also obtained from blend solutions of the precursor polymer and the organoclay Cloisite 30B for organoclay contents from 0 to 1.5 wt %.

The objective of this study was also to evaluate the effects of varying the equibiaxial stretching ratio on the oxygen permeation of transparent PI hybrid nanocomposites containing 1.0 wt % Cloisite 30B. We determined the optical transparencies and morphologies of the PI hybrid films for various equibiaxial stretching ratios. In this article, we report the rate of oxygen diffusion across PI hybrid films produced by equibiaxial stretching at various stretching ratios in the range 100–140%.

## EXPERIMENTAL

### Materials

Cloisite 30B (organically modified montmorillonite) was obtained from Southern Clay Products, Inc. (Tokyo, Japan) All reagents were purchased from TCI (Tokyo, Japan) and Aldrich Chemical Co. (Yongin, Korea). BTDA and BAPB were obtained from TCI and were used as received. DMAc was purified and dried over molecular sieves before use. All other reagents were used without further purification.

### Preparation of the PI hybrid film

Poly(amic acid) (PAA) was synthesized from BTDA and BAPB in DMAc under low-temperature conditions. BTDA (1.37 g, $5.57 \times 10^{-3}$ mol) and DMAc (10 mL) were placed in a three-necked, 100-mL flask, and the mixture was stirred at 0°C for 30 min under a nitrogen atmosphere. BAPB (1.63 g, $5.57 \times 10^{-3}$ mol) in DMAc (10 mL) was then added. The resulting solution was stirred vigorously at 0°C for 1 h and then at room temperature for 14 h; this yielded a 15 wt % DMAc solution of PAA.

The procedures used to prepare the polymer/organoclay hybrids were the same for all organoclay contents, so here we only describe the preparation of PI/Cloisite 30B (1.0 wt %) as a representative example. A dispersion of 0.03 g of Cloisite 30B, 3.0 g of PAA solution, and excess DMAc (10 mL) was stirred vigorously at room temperature for 2 h for better dispersion before heat treatment. Cloisite 30B was used for our hybrid systems because Cloisite 30B shows outstanding dispersability in DMAc. The solution was cast onto glass plates, and then, the solvent was evaporated at 50°C for 1 h. These films were dried in a vacuum oven at 80°C for 1 h. The film thickness was approximately 100 μm. The PAA films were further imidized on the glass plates through sequential heating at 110, 140, 170, 200, and 230°C for 30 min at each temperature with various pressure conditions and then for 30 min at 250°C. The chemical structures relevant to the synthetic route are shown in Scheme 1. We attempted to synthesize a PI hybrid film containing more than 1.5 wt % organoclay. However, repeated attempts to polymerize the 2.0 wt % Cloisite 30B/PI hybrid failed because of bubbles produced in the polymerization reactor. Excess organoclay in the PI hybrid containing 2.0 wt % Cloisite 30B appeared to prohibit production of the PI hybrid film.

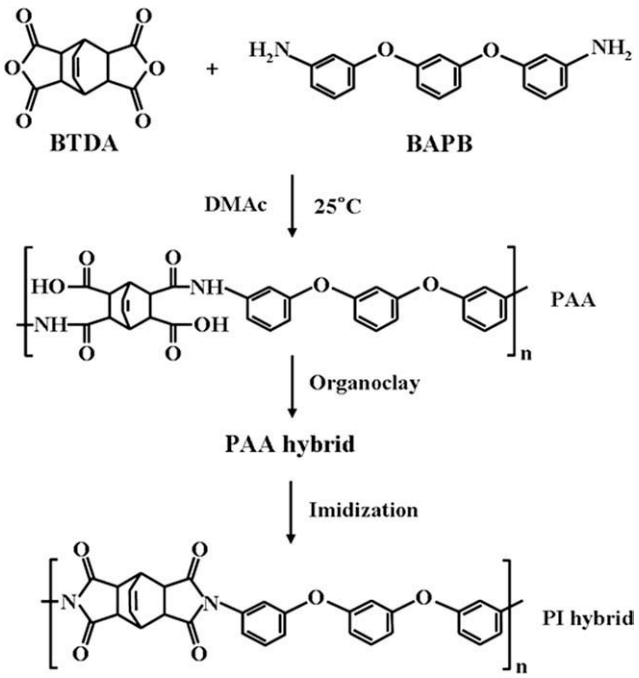


**Scheme 1** Synthetic route of the PI nanocomposite.

Table I lists the thermal imidization conditions employed in the preparation of the PI hybrid films. The PI was soluble in DMAc, which was the solvent used in the solution viscosity measurements. The inherent viscosities of the resulting PI hybrid films in DMAc were measured at a concentration of 0.1 g/dL at 30°C and found to range from 0.51 to 0.68 (see Table II). Considering that these viscosity values were obtained from pure PI in PI hybrids in which the clay contents had been removed, we regarded these numbers as being constant.

### Equibiaxial stretching of the PI hybrid film

The solvent-cast films were cut into sections with dimensions of 120 × 120 $mm^2$ (length × width). The films were then subjected to equibiaxial stretching with a biaxial stretching machine at stretching ratios in the range 100–140% and a strain rate of 1 mm/s at 220°C to obtain sheets 66–79 μm thick. Stretching temperatures exceeding 220°C were found to be excessive, and the obtained films tore and warped into wave structures.

**TABLE I**
**Thermal Heat Treatment Conditions for PAA and PI Films**

| Sample | Temperature (°C)/time (h)/pressure (Torr) |
|---|---|
| PAA | 0/1/760 → 25/14/760 |
| PAA hybrid | 25/2/760 → 50/1/760 → 80/1/1 |
| PI hybrid | 110/0.5/1 → 140/0.5/1 → 170/0.5/60 → 200/0.5/760 → 230/0.5/760 → 250/0.5/760 |

**TABLE II**
**Optical Transparencies of the PI Hybrid Films**

| Cloisite 30B in PI (wt %) | IV[a] | YI | $\lambda_o$ | 400 $nm_{trans}$ |
|---|---|---|---|---|
| 0 (pure PI) | 0.68 | 1.70 | 280 | 91 |
| 0.5 | 0.51 | 2.81 | 282 | 89 |
| 1.0 | 0.59 | 3.55 | 283 | 88 |
| 1.5 | 0.53 | 6.56 | 289 | 86 |

[a] Inherent viscosity measured at 30°C with a 0.1 g/100 mL solution in *N,N′*-dimethylacetamide.

Neat PI and the PI hybrid films were processed with the same method. No whitening of the hybrid films, which occurs sometimes in the stretching of films, was observed during the equibiaxial stretching. However, we were unable to obtain films with 150% stretching because of the nonuniformity of the film surfaces.

### Characterization

Fourier transform infrared (FTIR) spectra were obtained with an FTIR 460 instrument (Jasco, Tokyo, Japan) in the range 2000–1000 $cm^{-1}$ with KBr pellets. For all IR spectra, 36 co-added scans were collected at a special resolution of 2 $cm^{-1}$. Wide-angle X-ray diffraction (XRD) measurements were performed at room temperature on a Rigaku (D/Max-IIIB) X-ray diffractometer with Ni-filtered Cu-Kα radiation. The scanning rate was 2°/min over a range of 2θ of 2–32°.

TEM photographs of ultrathin sections of the PI hybrid films were obtained with a Leo 912 OMEGA transmission electron microscope (Tokyo, Japan) with an acceleration voltage of 120 kV. The color intensities of the polymer films were evaluated with a Minolta spectrophotometer (model CM-3500d). The ultraviolet–visible (UV–vis) spectra of the polymer films were recorded on a Shimadzu UV-3600 instrument (Tokyo, Japan). The $O_2$ permeabilities of the films were measured according to ASTM E 96 with a Mocon DL 100. The $O_2$ transmission rates were obtained at 23°C and at 1 atm of pressure.

## RESULTS AND DISCUSSION

### IR analysis

The formation of PAA and the completion of imide formation from amic acid were confirmed by examination of the FTIR spectra; the spectra of PAA and PI are shown in Figure 1. The C=O stretching peaks at 1700 and 1602 $cm^{-1}$ were due to the acid and amide groups of PAA, respectively, and shifted to higher frequencies in the imides, specifically to approximately 1782 $cm^{-1}$ (C=O, in phase) and 1712 $cm^{-1}$ (C=O, out of phase), respectively. In addition,

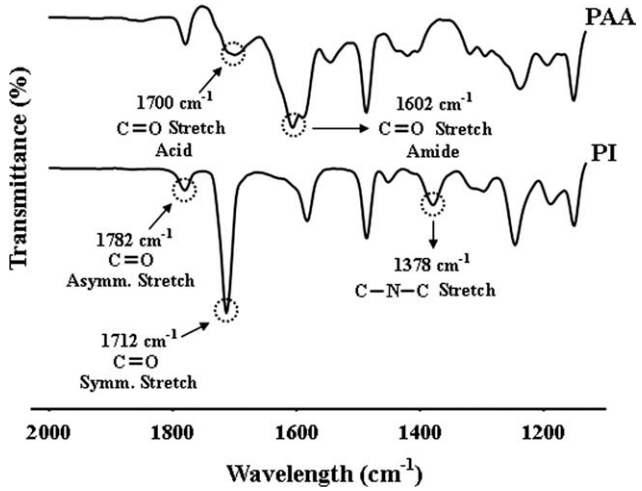


**Figure 1** FTIR spectra of PAA and PI.

the presence of a feature at 1378 $cm^{-1}$ corresponding to C—N—C stretching confirmed the formation of the imides.[35,36]

## Organoclay dispersion

Figure 2 shows the XRD curves for the organoclay, Cloisite 30B, in the region $2\theta = 2–32°$. The reflections of Cloisite 30B were found at $2\theta = 4.76°$ ($d = 18.58$ Å) and $2\theta = 20.00°$ ($d = 4.44$ Å). Figure 2 also shows the XRD curves of the pure PI and the PI hybrid films with various clay contents in the range 0–1.5 wt %. A broad peak at $2\theta = 16.67°$ ($d = 5.31$ Å) was found in the XRD pattern for pure PI. For the PI hybrids with 0.5–1.5 wt % Cloisite 30B, no obvious clay peaks were present in the XRD curves.

Figure 3 shows the XRD curves of the PI hybrid films containing 1.0 wt % Cloisite 30B for various

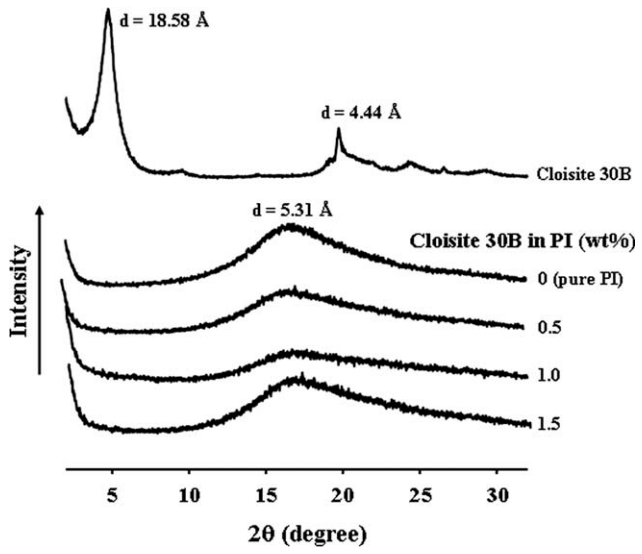


**Figure 2** XRD patterns of Cloisite 30B and PI hybrids with various Cloisite 30B contents.

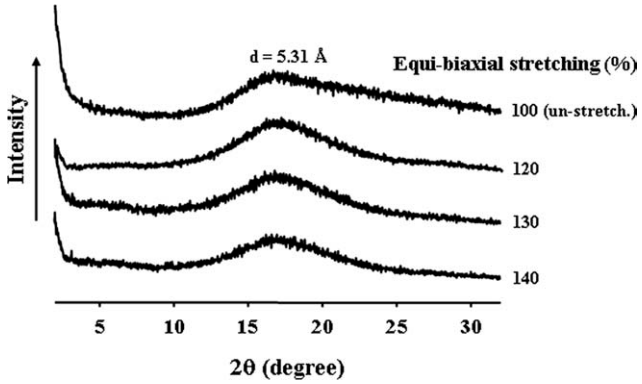


**Figure 3** XRD patterns of PI hybrid films containing 1.0 wt % Cloisite 30B with various equibiaxial stretching ratios.

equibiaxial stretching ratios in the range 100–140%. No obvious clay peaks in Figures 2 and 3 were also present in the XRD curves; this indicated that the clay layers in each of these hybrids were dispersed homogeneously in the PI matrix. This was direct evidence that the PI/Cloisite 30B hybrids formed nanocomposites.[37,38]

Although XRD allows for precise, routine measurements of clay layer spacings (1–4 nm), the spatial distributions of clay layers cannot be determined, nor can any structural inhomogeneities in the hybrids be detected. In addition, some layered clays do not initially exhibit well-defined basal reflections, so peak broadening and intensity decreases are difficult to follow systematically.[39,40] Therefore, conclusions concerning mechanisms of hybrid formation and hybrid microstructure based solely on XRD results are only tentative. Further evidence of the clay dispersion in the PI films on a nanometer scale was obtained with TEM.

## Morphology of the PI hybrid

We obtained more direct evidence of the formation of true nanocomposites by performing TEM on ultramicrotomed sections. Figures 4 and 5 show TEM photographs of the PI hybrid films containing 1.0 and 1.5 wt % Cloisite 30B, respectively. The dark lines in the photograph are the intersections of the 1 nm thick clay sheets, and the spaces between the dark lines are the interlayer spaces. Figure 4 shows the TEM image of a PI hybrid film containing 1.0 wt % Cloisite 30B. These clays were, for the most part, dispersed well in the polymer matrix, and some were agglomerated, but micrometer-scaled particles were not detected [see Fig. 4(b)]. The average particle was below 10 nm in thickness, as calculated from the TEM photographs; this confirmed the formation of nanocomposites. Figure 5 shows that the clay layers were also well dispersed in the polymer matrix of the PI hybrid containing 1.5 wt % organoclay,

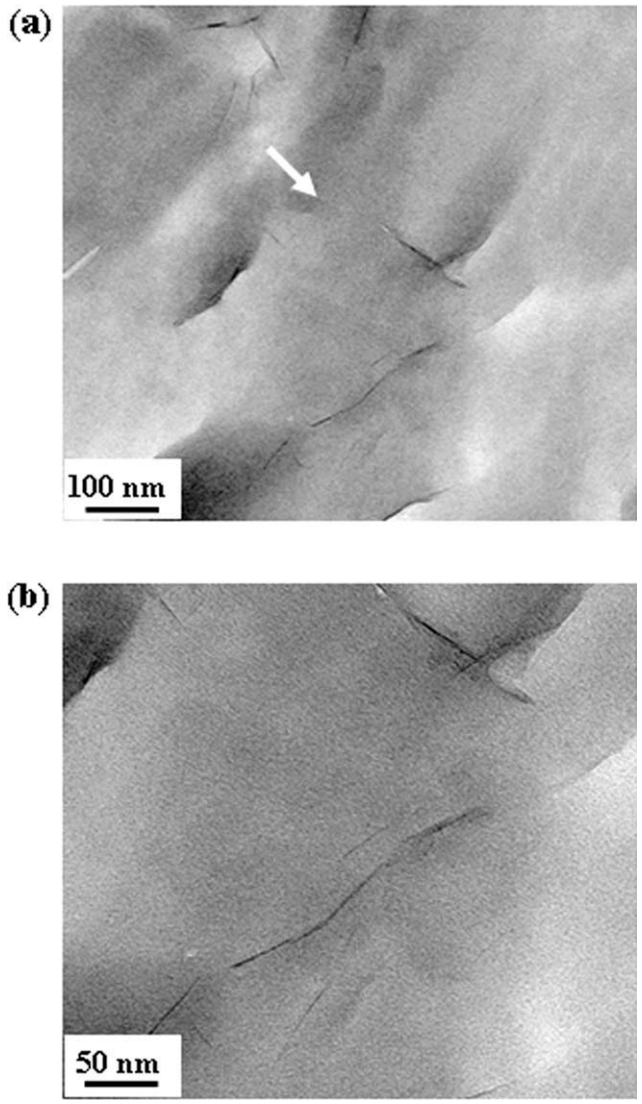


**Figure 4** TEM micrographs of 1.0 wt % Cloisite 30B in PI hybrid films with increasing magnification levels from (a) to (b).

although some clusters or agglomerated particles with sizes in the range 10–20 nm were also be detected [see Fig. 5(b)], so there was more agglomeration in this hybrid than in the PI hybrid containing 1.0 wt % organoclay. These results confirmed that the clay in our hybrids was broken down into nanoscale building blocks and dispersed homogeneously in the polymer matrices to afford PI/clay nanocomposites.

TEM photographs of PI hybrid films with equibiaxial stretching ratios from 120 to 140% are shown in Figure 6. Stretching ratios of 120% or greater yielded clay layers that were exfoliated and dispersed randomly in the PI matrix. Figure 6(a–c) shows TEM photographs of the PI hybrid films containing 1.0 wt % organoclay with equibiaxial stretching from 120 to 140%. These TEM photographs show that most of the clay layers were exfoliated and dispersed homogeneously in the PI matrix. The XRD profiles in Figure 3 also show that the clay layers were well dispersed in the PI hybrids, as discussed previously.

### Optical transparency

The optical properties of the PI hybrid films with various Cloisite 30B contents are listed in Table II. Table II shows that the color intensities of the PI hybrid films were affected by their organoclay content and also that the PI hybrid films with lower organoclay contents had lower yellow index (YI) values than the hybrids with higher organoclay contents. The YI value of the PI hybrid with 0.5 wt % organoclay was 2.81; when the clay loading was increased to 1.0 and then to 1.5 wt %, there were significant increases in the YI value, to 3.55 and 6.56, respectively. However, these values of YI were

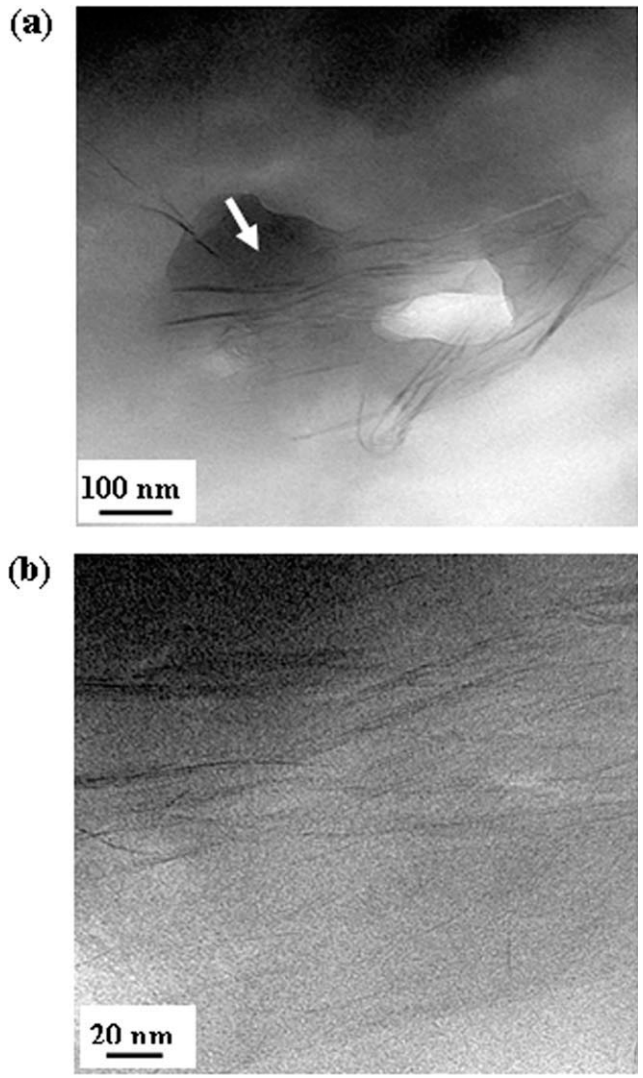


**Figure 5** TEM micrographs of 1.5 wt % Cloisite 30B in PI hybrid films with increasing magnification levels from (a) to (b).

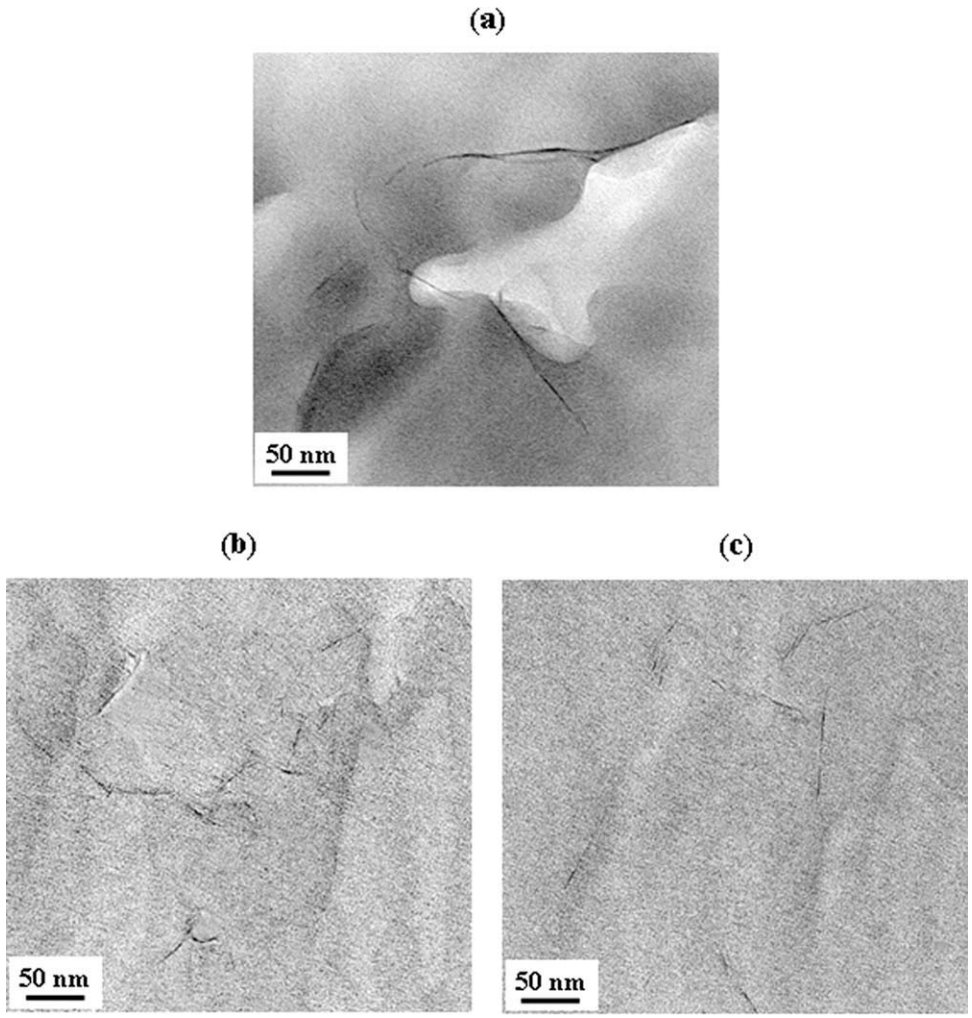


**Figure 6** TEM micrographs of PI hybrid films containing 1.0 wt % Cloisite 30B with various equibiaxial stretching ratios: (a) 120, (b) 130, and (c) 140%.

much lower than those of conventional aromatic PI films, such as Kapton 200KN (YI = 97.50).[41]

The color intensities of the hybrid films were also determined from the $\lambda_o$ values in the UV–vis absorption spectra, as shown in Table II. The $\lambda_o$ values of the PI hybrids increased slightly with the organoclay loading, from 280 to 289 nm, when the Cloisite 30B content was increased from 0 to 1.5 wt %. These colorless PI hybrid films exhibited a high level of UV transmittance, almost 85% at 400 nm, and excellent optical properties (see Fig. 7). The solvent-cast films of the hybrids with organoclay contents in the range 0–1.5 wt % were all almost colorless and transparent, as shown in Figure 8(a–d); this indicated that the addition of the organoclay to the PI matrix did not significantly affect its transparency. These findings suggest that, even at an organoclay loading of 1.5 wt %, the phase domains in the hybrid film were significantly smaller than the wavelength of visible light.[42,43] Thus, the hybrid films prepared in this study exhibited excellent transparency because of the good dispersion of clay particles in the polymer matrix, although the transparency did diminish slightly with increasing organoclay content because of the agglomeration of the clay particles.

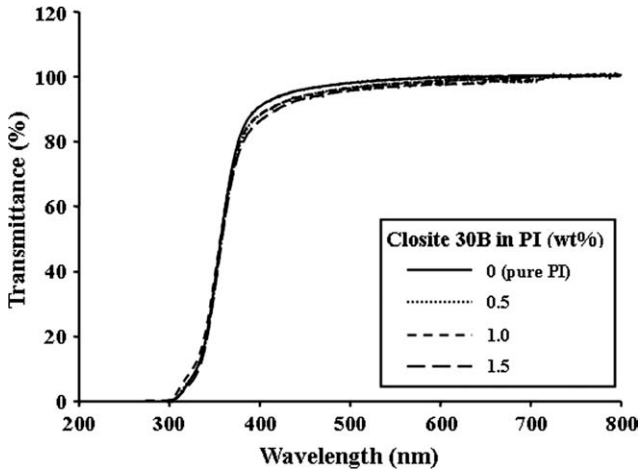


**Figure 7** UV–vis transmittance (%) of PI hybrid films with various Cloisite 30B contents.

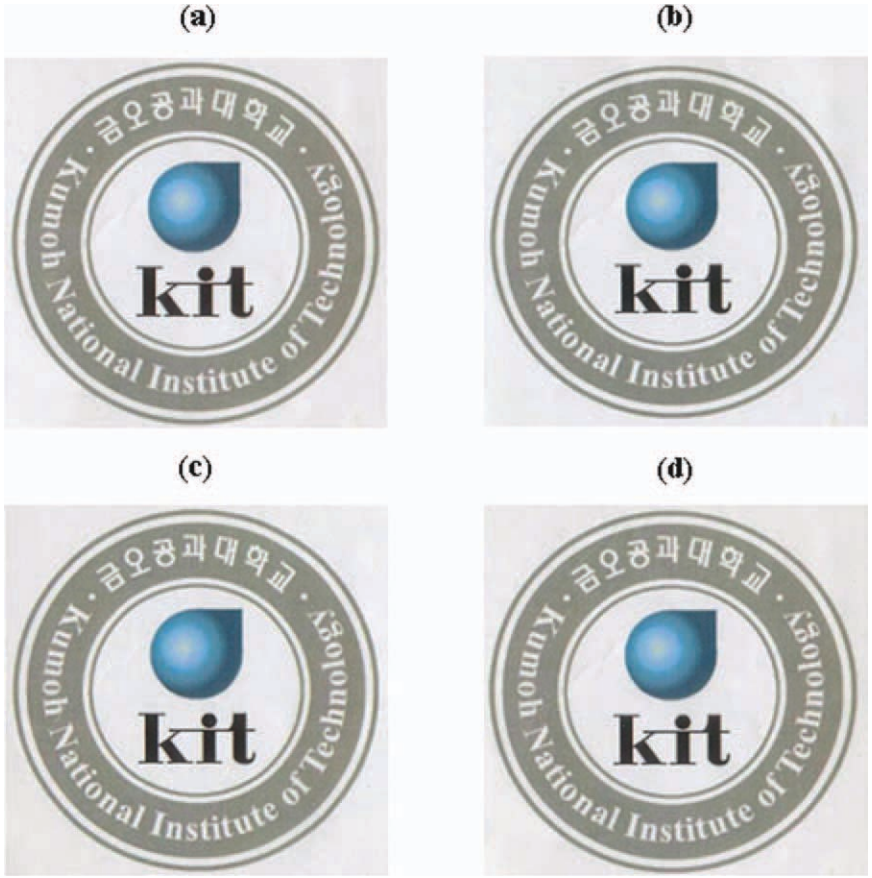


**Figure 8** Photographs of PI hybrid films containing (a) 0 (pure PI), (b) 0.5, (c) 1.0, and (d) 1.5 wt % Cloisite 30B. [Color figure can be viewed in the online issue, which is available at wileyonlinelibrary.com.]

The optical properties of the PI hybrid films with various stretching ratios are listed in Table III. Table III shows that the value of YI of the unstretched PI hybrid film was 3.55. When the stretching ratio was increased to 120% and then to 140%, the YI values for the PI hybrid films were found to be fairly constant, increasing to 3.56 and 3.67, respectively.

The color intensities of the hybrid films were determined by examination of the $\lambda_o$ values of their UV–vis absorption spectra. Figure 9 shows the UV–vis spectra of the PI hybrid films with various stretching ratios, which were recorded in the range 283–291 nm for stretching ratios of 100–140% (Table III). These colorless PI hybrid films exhibited a high level of UV transmittance, almost 85% at 400 nm, and excellent optical properties (see Table III).

**TABLE III**
**Optical Transparencies of PI Hybrid Films Containing 1 wt % Organoclay with Various Equibiaxial Stretching Ratios**

| Equibiaxial stretching (%)[a] | YI | $\lambda_o$ (nm) | 400 $nm_{trans}$ |
|---|---|---|---|
| 100 (unstretched) | 3.55 | 283 | 88 |
| 120 | 3.62 | 285 | 86 |
| 130 | 3.67 | 291 | 87 |
| 140 | 3.56 | 290 | 86 |

[a] Equibiaxial stretching at 220°C with a 1 mm/s draw speed.

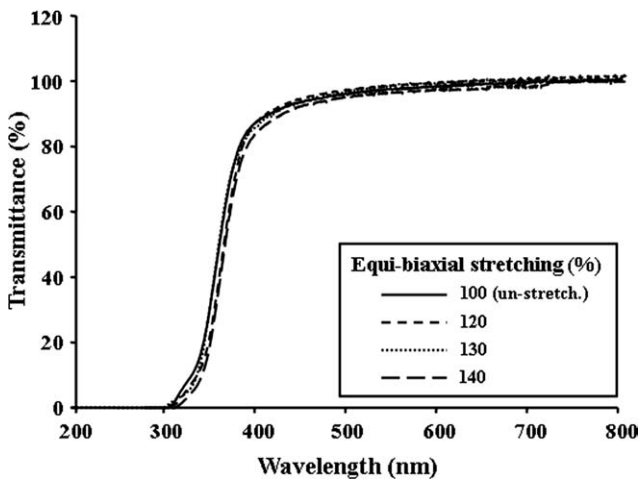


**Figure 9** UV–vis transmittances of PI hybrid films containing 1.0 wt % Cloisite 30B with various equibiaxial stretching ratios.

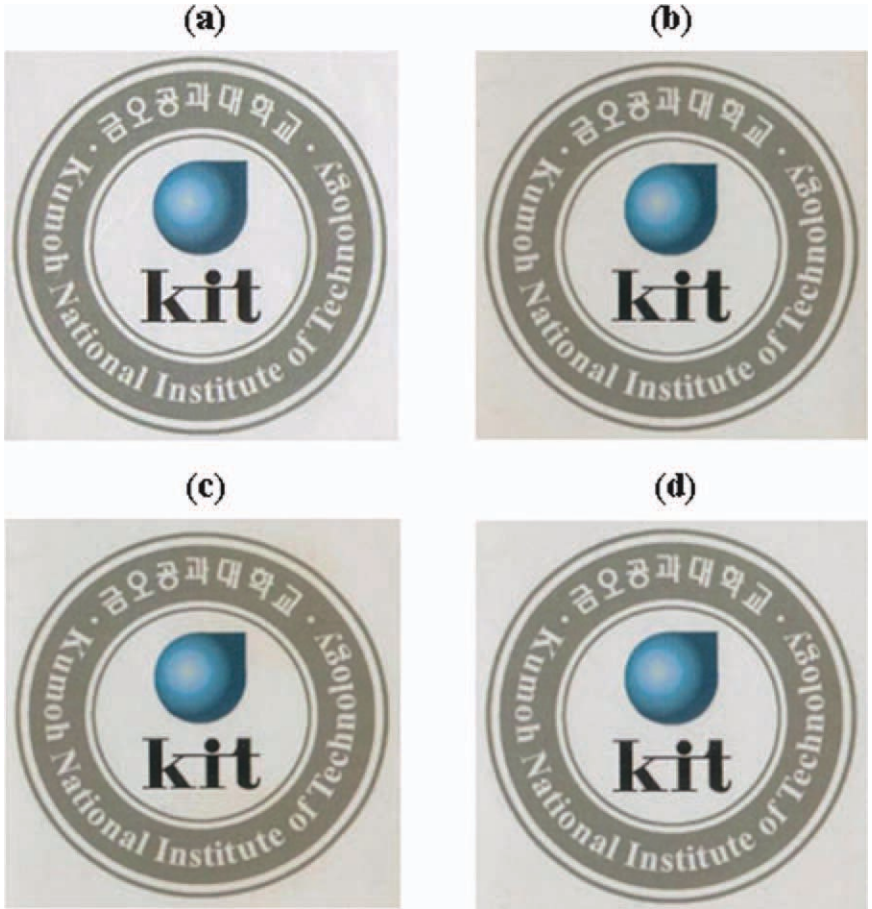


**Figure 10** Photographs of PI hybrid films containing 1.0 wt % Cloisite 30B with various equibiaxial stretching ratios: (a) 100 (unstretched), (b) 120, (c) 130, and (d) 140%. [Color figure can be viewed in the online issue, which is available at wileyonlinelibrary.com.]

The solvent-cast hybrid films with equistretching ratios in the range 100–140% were all almost transparent, as shown in Figure 10(a–d); this indicated that the variation of the stretching of the PI matrix did not significantly affect their transparency. The hybrid films prepared in this study exhibited excellent transparency because the clay particles were well dispersed in the polymer matrix.

## Oxygen permeability

Models of the gas permeability of polymer composites must account for the shape and spatial orientation of the dispersed phase. The gas permeability of composites consisting of filler particles dispersed in a polymer matrix has been predicted in several studies.[27,28,44,45] The reduction in the gas permeability arising from a clay with a platelet morphology is significantly better than for an agglomerated droplet nanocomposite morphology. The mobility of the polymer chain segments in a polymer nanocomposite is obviously different from that in the pure polymer because of their confined environment, which affects the gas permeability. There are two main factors affecting the permeability reduction, namely, the polymer chain-segment immobility and the *detour ratio,* which is defined as the ratio of the film thickness in the nominal diffusion flow direction to the average length of the tortuous diffusion distance between the clay layers.[46–48]

In this study, we explored the performance of barrier films containing aligned impermeable particles. In this article, we discuss our results in terms of the relative permeability ($P_c/P_p$, where $P_p$ is the permeability of the pure polymer and $P_c$ is the

**TABLE IV**
**Oxygen Permeations of PI Hybrid Films with Various Organoclay Contents**

| Cloisite 30B in PI (wt %) | Film thickness (μm) | $O_2$TR (cc/m$^2$/day)[a] | $P_c/P_p$ |
|---|---|---|---|
| 0.0 (pure PI) | 68 | 1.202 | 1.00 |
| 0.5 | 64 | 0.897 | 0.75 |
| 1.0 | 66 | 0.203 | 0.17 |
| 1.5 | 65 | 0.340 | 0.28 |

[a] Oxygen transmission rate.

**TABLE V**
**Oxygen Permeations of PI Hybrid Films Containing 1.0 wt % Organoclay with Various Equibiaxial Stretching Ratios**

| Equibiaxial stretching (%)[a] | Film thickness (μm) | $O_2$TR (cc/m$^2$/day)[b] | $P_c/P_p$ |
|---|---|---|---|
| 100 (unstretched) | 3.55 | 283 | 88 |
| 120 | 3.62 | 285 | 86 |
| 130 | 3.67 | 291 | 87 |
| 140 | 3.56 | 290 | 86 |

[a] Equibiaxial stretching at 220°C with a 1 mm/s draw speed.
[b] Oxygen transmission rate.

permeability of the composite). The oxygen permeability values for hybrid films with clay loadings of 0–1.5 wt % are summarized in Table IV. The permeability coefficient of the 1.0 wt % PI hybrid film was 83% (0.203 cc/m$^2$/day) lower than that of the pure PI film. This reduced permeability was due to the presence of dispersed clay layers with large aspect ratios in the polymer matrix, as has been shown for other nanocomposites.[49,50] When, however, the organoclay content reached 1.5 wt %, the oxygen permeability increased to 0.340 cc/m$^2$/day. This increase in the permeation was mainly due to agglomeration of the clay particles above a critical clay content (see Fig. 5).

The PI hybrid film containing 1.0 wt % Cloisite 30B exhibited the best oxygen barrier properties, so the permeabilities of $O_2$ through various PI hybrid films containing 1.0 wt % Cloisite 30B with different equibiaxial stretching ratios were determined and are presented in Table V. For biaxial stretching ratios between 100 and 130%, the oxygen permeabilities of the PI hybrid films were found to decrease linearly from 0.203 to 0.027 cc/m$^2$/day (an 87% reduction). This trend could be attributed to the lengthening upon stretching of the tortuous diffusion paths traversed by the gas molecules through the film matrix and to the interactions between the oxygen and clay molecules. Furthermore, films subjected to higher stretching ratios appeared to be much more rigid; this would also be expected to contribute to decreases in their gas permeabilities.[51,52] However, when the biaxial stretching ratio reached 140%, the oxygen permeability increased to 0.156 cc/m$^2$/day (a 23% reduction). This increase in the permeability of $O_2$ seemed to be due to excessive biaxial stretching and the resulting formation of microsized pinholes in the hybrid films.

## CONCLUSIONS

In this study, we focused on the synthesis of new transparent PI/Cloisite 30B hybrid films by using the *in situ* solution intercalation method via PAA. The clay contents of the nanohybrid films were varied from 0.5 to 1.5 wt %, and the effects on the optical properties, morphologies, and gas permeabilities of the films were examined. The morphological studies indicated that the dispersion in the PI matrix was better at a lower organoclay loadings than at a higher organoclay loading. For low clay contents (1.0 wt %), the clay particles were well dispersed in the matrix polymer without a significant agglomeration of particles. Optimum barrier properties were observed for the hybrids containing 1.0 wt % Cloisite 30B. The values of YI were found to vary from 1.70 to 6.56 with increases in the organoclay content from 0 to 1.5 wt %. Our UV–vis measurements showed that the PI hybrid films had excellent transparency, which decreased only slightly with increases in the organoclay content.

PI hybrid films containing 1.0 wt % Cloisite 30B were equibiaxially stretched over the range 100–140% at 220°C. The variations with the equibiaxial stretching ratio in the optical transparency and gas permeability of the hybrid films were analyzed. PI hybrid films with 130% biaxial stretching were found to exhibit the best improvements in $O_2$ barrier properties. In this study, equibiaxial stretching was found to be very effective at improving the oxygen barrier properties of PI nanocomposite films. However, the optical transparencies were found to be almost independent of variation in the equibiaxial stretching ratio.

## References


1. Chung, C.-L.; Hsiao, S.-H. Polymer 2008, 49, 2476.
2. Wang, H.-W.; Dong, R.-X.; Chu, H.-C.; Chang, K.-C.; Lee, W.-C. Mater Chem Phys 2005, 94, 42.
3. Wang, X. L.; Li, Y. F.; Gong, C. L.; Ma.T.; Yang, F. C. J Fluor Chem 2008, 129, 56.
4. Ge, Z.; Fan, L.; Yang, S. Eur Polym J 2008, 44, 1252.
5. Hsiao, S. H.; Chen, Y. J. Eur Polym J 2002, 38, 815.
6. Hasegawa, M.; Horiuchi, M.; Wada, Y. High Perform Polym 2007, 19, 175.
7. Li, T. L.; Hsu, S. L. C. Eur Polym J 2007, 43, 3368.
8. Zhao, X.; Lin, J.; Yang, H.; Fan, L.; Yang, S. Eur Polym J 2008, 44, 808.
9. Hasegawa, M.; Horie, K. Prog Polym Sci 2001, 26, 259.
10. Omote, T.; Yamaoka, T.; Koseki, K. J Appl Polym Sci 1989, 38, 389.
11. Xu, J. W.; Chung, M. L.; Chung, T. S.; He, C. B.; Wang, R. Polymer 2003, 44, 4715.
12. Jang, W.; Shin, D.; Choi, S.; Park, S.; Han, H. Polymer 2007, 48, 2130.
13. Ma, S. L.; Kim, Y. S.; Lee, J. H.; Kim, J. S.; Kim, I.; Won, J. C. Polym (Korea) 2005, 29, 204.
14. Yang, C. P.; Su, Y. Y.; Wen, S. J.; Hsiao, S. H. Polymer 2006, 47, 7021.
15. Yang, C. P.; Su, Y. Y. Polymer 2005, 46, 5778.
16. Yang, C. P.; Hsu, S. L. C.; Chen, J. S. J Appl Polym Sci 2005, 98, 2064.
17. Choi, I. H.; Chang, J.-H. Polym (Korea) 2010, 34, 480.
18. Min, U.; Chang, J.-H. Polym (Korea) 2010, 34, 495.

19. Jang, W.; Shin, D.; Choi, S.; Park, S.; Han, H. Polymer 2007, 48, 2130.
20. Li, F.; Fang, S.; Ge, J. J.; Honigfort, P. S.; Chen, J. C.; Harris, F. W.; Cheng, S. Z. D. Polymer 1999, 40, 4571.
21. Jin, H.-S.; Chang, J.-H. J Appl Polym Sci 2008, 107, 109.
22. Ghosal, K.; Freeman, B. D.; Chern, R. T.; Alvarez, J. C.; De la Camoa, J. G.; Lozano, A. E.; De Abajo, J. Polymer 1995, 36, 793.
23. Maiti, P.; Yamada, K.; Okamoto, M.; Ueda, K.; Okamoto, K. Chem Mater 2002, 14, 4654.
24. Joly, C.; Smaihi, M.; Porcar, L.; Noble, R. D. Chem Mater 1999, 11, 2331.
25. Ebeling, T.; Norek, S.; Hasan, A.; Hiltner, A.; Baer, E. J Appl Polym Sci 1999, 71, 1461.
26. Jarus, D.; Hiltner, A.; Baer, E. Polymer 2002, 43, 2401.
27. Bharadwaj, R. K. Macromolecules 2001, 34, 9189.
28. Nielson, L. E. J. Macromol Sci Chem 1967, 5, 929.
29. Mittal, V. Barrier Properties of Polymer Clay Nanocomposites; Nanotech Sci Tech Series; Nova Science: New York, 2009; p 73.
30. Coolier, J. R. Ind Eng Chem 1969, 61, 72.
31. Fan, G.; Di Maio, L.; Incarnato, L.; Scarfato, P.; Acierno, D. Packag Technol Sci 2000, 13, 123.
32. Jeol, S.; Fenouillot, F.; Rousseau, A.; Masenelli-Varlot, K.; Gauthier, C.; Briois, J. F. Macromolecules 2007, 40, 3229.
33. Perrin-Sarazin, F.; Ton-That, M.-T.; Bureau, M. N.; Denault, J. Polymer 2005, 46, 11624.
34. Morgan, A. B.; Gilman, J. W. J Appl Polym Sci 2003, 87, 1329.
35. Saeed, M. B.; Zhan, M. S. Eur Polym J 2006, 42, 1844.
36. Pavia, D. L.; Lampman, G. M.; Kriz, G. S. Introduction to Spectroscopy; Harcourt: Washington, DC, 2001; Chapter 2.
37. Liang, Z. M.; Yin, J.; Wu, J. H.; Qiu, Z. X.; He, F. F. Eur Polym J 2004, 40, 307.
38. Davis, C. H.; Mathias, L. J.; Gilman, J. W.; Schiraldi, D. A.; Shields, J. R.; Trulove, P.; Sutto, T. E.; Delong, H. C. J Polym Sci Part B: Polym Phys 2002, 40, 2661.
39. Vaia, R. A.; Jandt, K. D.; Kramer, E. J.; Giannelis, E. P. Chem Mater 1996, 8, 2628.
40. Galgali, G.; Ramesh, C.; Lele, A. Macromolecules 2001, 34, 852.
41. Hasegawa, M.; Horie, K. Prog Polym Sci 2001, 26, 259.
42. Chang, J.-H.; Park, D. K.; Ihn, K. J. J Appl Polym Sci 2002, 84, 2294.
43. Yano, K.; Usuki, A.; Okada, A.; Kurauchi, T.; Kamigaito, O. J Polym Sci Part A: Polym Chem 1993, 31, 2493.
44. Ju, C. H.; Kim, J.-C.; Chang, J.-H. J Appl Polym Sci 2007, 106, 4192.
45. Ray, S. S.; Okamoto, M. Prog Polym Sci 2003, 28, 1539.
46. Petropoulos, J. H. Adv Polym Sci 1985, 64, 93.
47. Chaiko, D. J.; Leyva, A. A. Chem Mater 2005, 17, 13.
48. Cristian, C. F.; Manuel, A. V. J Polym Sci Part B: Polym Phys 2005, 43, 2625.
49. Xu, B.; Zheng, Q.; Song, Y.; Shangguan, Y. Polymer 2006, 47, 2904.
50. Sakaya, T.; Osaki, N. J Photopolym Sci Technol 2006, 19, 197.
51. Rajeev, R. S.; Harkin-Jones, E.; Soon, K.; McNally, T.; Menary, G.; Armstrong, C. G.; Martin, P. J. Eur Polym J 2009, 45, 332.
52. Ke, Y.; Long, C.; Qi, Z. J Appl Polym Sci 1999, 71, 1139.